phys. stat. sol. (b) **245**, No. 9, 1849–1857 (2008) / **DOI** 10.1002/pssb.200879538

physica status solidi b
www.pss-b.com
basic solid state physics

Niobium-doped TiO_2 films as window layer for chalcopyrite solar cells

Bernhard Neumann*, Frauke Bierau, Benjamin Johnson, Christian Alexander Kaufmann, Klaus Ellmer, and Helmut Tributsch

Hahn Meitner Institut, Solar Energy Department, Glienickerstr. 100, 14109 Berlin, Germany

Received 8 February 2008, revised 30 June 2008, accepted 1 July 2008
Published online 11 August 2008

Dedicated to Prof. Helmut Tributsch on the occasion of his 65th birthday

PACS 73.50.Dn, 78.30.Hv, 78.40.Ha, 81.15.Cd, 84.60.Jt

* Corresponding author: e-mail bernhard.neumann@hmi.de, Neumann@johanna-solar.com, Phone: +49-30-8062-2508, Fax: +49-30-8062-2434

Smooth and semitransparent $Nb_xTi_{1-x}O_y$ ($x = 0.03$, $y = 1.84-1.91$) films have been prepared by reactive magnetron sputtering at temperatures below 420 K. Structural investigations by RAMAN-spectroscopy together with resistivity- and temperature-dependent Hall-measurements were used in order to analyze the film structure and the nature of the charge transport in this material. These films can be used as a window layer (TCO) for thin film solar cells. $Cu(In,Ga)Se_2$ solar cells equipped with the new window layer keep their functionality which excludes first, the presence of strong energetic barriers and second, a strong interfacial recombination. The development of TiO_2-based window layers is expected to make thin film solar cells less sensitive against corrosion after contact with humidity.

1 Introduction Transparent conducting oxides (TCO) play an important role in optoelectronic devices. Tin-doped indium oxide (ITO) is widely used in flat panel displays and aluminium-doped zinc oxide (Al:ZnO) as window- and contact layers in several types of thin film solar cells [1–3]. After long-term development, both materials show excellent properties in terms of transparency and conductivity. But the strong increase of the world market price of indium [4] and the known instability of ZnO against moisture [5, 6] require new materials with additional functional properties, like an improved corrosion stability, for instance. One promising new candidate as a TCO-material is niobium-doped titanium dioxide, recently investigated by Furubayashi et al. [7]. $Nb_xTi_{1-x}O_2$ ($x = 0.02-0.2$) films prepared by pulsed laser deposition (PLD) from sintered TiO_2/Nb_2O_5-targets show a transparency better than 90% for 40 nm thick films and a resistivity as low as $3 \times 10^{-4}\ \Omega$ cm. This is comparable to aluminium or gallium doped ZnO-films, which typically show resistivities of about $5 \times 10^{-4}\ \Omega$ cm to $1 \times 10^{-3}\ \Omega$ cm [8]. However, for an application in thin film solar cells the high deposition temperature of 820 K would cause problems in cation-diffusion and this technique has thus been so far excluded. With the help of reactive magnetron sputtering, transparent and conductive $Nb_xTi_{1-x}O_2$-films with similar stoichiometries have been prepared at deposition temperatures below 420 K.

Titanium dioxide (TiO_2) as a TCO-host material is interesting because it has several favourable properties. The transparency for visible light is given due to the large band gap of 3.0 eV and 3.2 eV for rutile and anatase crystals, respectively [9, 10]. The within the Anderson model estimated conduction band discontinuity between the front electrode and cadmiumsulfide (CdS) buffer layer in the hetero-junction of an $Cu(In,Ga)Se_2$-solar cell is only marginally higher for TiO_2-films than for ZnO-films. By taking an electron affinity of 4.21 eV for TiO_2, 4.19 eV for ZnO and 3.9 eV for CdS [11], a conduction band discontinuity of 0.31 eV is calculated for the TiO_2/CdS-interface and of 0.29 eV for the ZnO/CdS-interface. Contrary to zinc oxide, TiO_2 benefits from an extraordinary chemical- and photocorrosion stability and the material is relative abundant, too. Unfortunately, intrinsic TiO_2-films show a high resistivity of about $1 \times 10^6\ \Omega$ cm [10, 12]. Ways to vary the electronic properties of TiO_2-films are doping with cations and the introduction of oxygen vacancies by vacuum annealing or partial reduction.

The reactive magnetron sputtering process, a plasma-based film deposition method, can be controlled by the parameters plasma energy, sputter pressure, substrate temperature, partial pressure of the reactive gas and the distance from the target to the substrate. All parameters mentioned have an influence on the concentration and the kinetic energy of the sputtered atoms and thus affect the film growth and especially its crystallinity [13]. Thornten et al. described these effects in detail [14]. As a consequence, films sputtered at low temperatures and high (plasma)-energies often exhibit small grain sizes (<5–10 nm) and show an increased number of defect sites and lattices stress [15, 16], which may be disadvantageous for electronic applications, due to an increase in grain boundary effects [3].

The plasma used for the sputtering process can be maintained by a direct current supply (DC) or by a radio frequency-technique, typically named as RF-sputtering. The ladder is preferred in case of low conductive metaloxide-targets, whereas the first mentioned method is applicable for both pure metallic and for extraordinary conductive metaloxide-targets. In general, the use of a metallic-target in combination with a reactive gas, like oxygen (metaloxides), carbon-monoxide (metalcarbides) or nitrogen (metalnitrides), provides a more flexible variation of the reactive-gas-content in the deposited layer, than an already pre-synthesised metaloxide-compound-target for instance does. But in case of reactive DC-sputtering from a metallic target, it is important to control the sputtering-process exactly, due to the weak expressed balance between the sputtering from a origin, pure metallic target surface and the sputtering from an already with the process-gas reacted metal-target-surface.

According to the work of Wang et al. [15], Karunagaran et al. [16], Löbl et al. [17] and Lee et al. [18], the degree of crystallinity, the type of TiO_2-phases (anatase, rutile) and the TiO_2 particle size depend mostly on the deposition temperature and the kinetic energy of the impinging particles. The lowest deposition temperature for obtaining crystalline TiO_2-films were found by Löbl et al. with temperatures of about 320–370 K [17].

Niobium-doped TiO_2-films were investigated by Furubayashi [7], Ruiz [19], Valigi [20], Sheppard [21] and Pehlivan et al. [22] with respect to optical and electronical properties and basic research in film structure and morphology. According to the work of Sheppard, the TiO_2-lattice enlarges linearly with increasing Niobium concentration, fulfilling Vegards law [23]. Up to a doping concentration of about 40 at% Niobium no phase separation took place [21]. The nature of defect states in the Nb:TiO_2-films, especially for vacuum processed ones, was discussed by Ruiz and Valigi et al. in detail [19, 20]. Their results will be referred to later in the discussion part of this article. In the following, the preparation of conductive and semitransparent $Nb_{0.03}Ti_{0.97}O_{1.84}$-films by reactive magnetron sputtering at temperatures below 420 K will be described and their investigation as a new window- and contact for thin film Cu(In,Ga)Se_2 solar cells presented.

2 Experimental

2.1 Film preparation Nb:TiO_2 films were prepared by reactive magnetron sputtering in an argon/oxygen atmosphere from both a metallic titanium and an alloyed metallic titanium–niobium-target containing 6 wt% niobium (FHR-Dresden, Ø: 76 mm). The plasma is sustained by direct current (DC, 25 kHz) at a constant power of 200 W. Unless indicated, the sputtering pressure was kept at 0.6 Pa. The distance between target and substrate was 6.5 cm. The oxygen flow rate was varied between 2.7 sccm and 3.4 sccm by a mass flow controller, while the argon flow rate was adapted to fix the total gas flow at 50 sccm. The substrate was heated from the rear with a halogen-lamp (150 W, Osram HLX-64635). The temperature, controlled with a Ni/Cr thermocouple, was kept between 400 K and 420 K. In a typical deposition experiment, the target was intensively conditioned under a "metallic" modus, before the O_2-flow was stepwise increased until the desired working point/discharge voltage was reached. During the relative short deposition time of 5 to 10 minutes, the discharge voltage was kept constant by small variations of the O_2-flow rate by hand. With decreasing oxygen flow during deposition, the film growth rate increased from 0.33 nm s^{-1} (1.66 nm s^{-1} kW^{-1}) to 1 nm s^{-1} (5 nm s^{-1} kW^{-1}). For resistivity measurements and spectroscopic analyses, thin films were deposited at bare float glass substrates (22 × 22 mm). The film compositions was determined qualitatively and quantitatively by elastic recoil detection analysis (ERDA). In order to minimize oxygen-contamination from the substrate, freshly etched silicon wafers were used in this case (100-orientation, 4% aqueous HF solution, 4 min etching time). For solar cell experiments, standard Cu(In,Ga)Se_2-layers prepared on molybdenum-coated, flexible titanium-foil, with a cadmiumsulfide buffer-layer (CdS), were covered with ZnO- (standard cells) and with the $Nb_{0.03}Ti_{0.97}O_{1.84}$-films, respectively, in order to investigate the electronic behaviour of the new window layer in the heterojunction. The preparation of the Cu(In,Ga)Se_2-layers is described elsewhere [24]. In the standard solar cells, the front contact consists of an intrinsic (i-ZnO) and an aluminium-doped zinc oxide layer (Al:ZnO, total thickness ZnO: ~500 nm) and a nickel–aluminium-grid for improving the lateral charge collection (d: 1 µm, R_{sheet}: 0.27 Ω cm^{-2}), whereas in the $Nb_{0.03}Ti_{0.97}O_{1.84}$-window layer equipped cells (d: 150–250 nm) a titanium-grid (d: 200 nm, R_{sheet}: 48 Ω cm^{-2}) was used.

2.2 Film and solar cell characterization The thickness of the films was measured by a profilometer (DEKTAK 8). Resistance measurements were performed either in a 2- or in a 4-contact geometry with a Keithly 616 Elektrometer, after evaporation of lateral titanium-contact-stripes (200 nm) on the films. In order to determine charge

carrier concentrations, charge carrier mobilities and charge transport activation energies in the $Nb_xTi_{1-x}O_y$-films, temperature dependend Hall-measurements were performed (Keithley DMM19/705; 0.85 Tesla, van der Pauw-analyzing method). The X-ray diffraction measurements were carried out with a Siemens diffractometer D500/5000 in Bragg–Brentano geometry with Cu K_α-radiation. Raman-measurements were performed with an inverse microscope, equipped with a He–Ne-laser (632 nm) and the following optical setup: 100-objective, slit width 100 µm, confocal hole of 1000 µm diameter, a 1800-interference-grating (gr/mm), a notch-filter and a CCD-camera. The laser intensity of about 2 mW used in the experiments did not induce changes in the films. The spectral resolution is estimated to be better than 0.5 cm^{-1}. The morphology of the films was studied additionally by scanning electron microscopy (SEM, LEO44). The optical characterization was done by measuring the transmission and reflection of the films with the help of a Cary 2000 spectrometer including an Ulbricht-sphere. The elastic recoil detection analysis was done at the Hahn–Meitner institute Berlin with accelerated gold ions (350 MeV) using an angle of incidence of 15°. The analyzed elements and their relative errors in the measured atom-concentrations were estimated to be ±2% for titanium, ±5% for niobium, ±2% for oxygen, ±10% for sodium and ±10% for argon. The performance of the solar cells was measured with a sun simulator (1000 W Xe-lamp, Oriel, AM 0 and AM 1.5 filter, 100 mW cm^{-2}, Si-reference cell) at room temperature (293 K, active cooling system) including a 4-point measuring system.

3 Results

3.1 Structural characterisation of the $Nb_xTi_{1-x}O_y$-films With an increasing oxygen flow-rate from 3.25 sccm to >3.35 sccm the Nb/Ti-ratio did not change significantly (0.033–0.035, Table 1), while the metal/oxygen-ratio decreased from 0.55 to 0.52. The TCO-like niobium-doped titanium oxide films show a composition of $Nb_{0.03}Ti_{0.97}O_{1.84}$. Annealing of the $Nb_{0.03}Ti_{0.97}O_{1.84}$-films at 720 K in air led the oxygen content to increase significantly (Table 1). Contamination with argon- and chlorine-atoms in the layers was low with estimated values of about 0.27 at% and 0.15 at%, respectively.

The thermally untreated $Nb_{0.03}Ti_{0.97}O_{1.84}$-films were X-ray amorphous, which may be caused by an absence of crystalline phases of a sufficient size (~5 nm). Therefore, Raman spectroscopy was performed to investigate the film structure, since it is known to be more sensitive. Table 2 gives an overview of expected Raman-modes of Ti_xO_y-

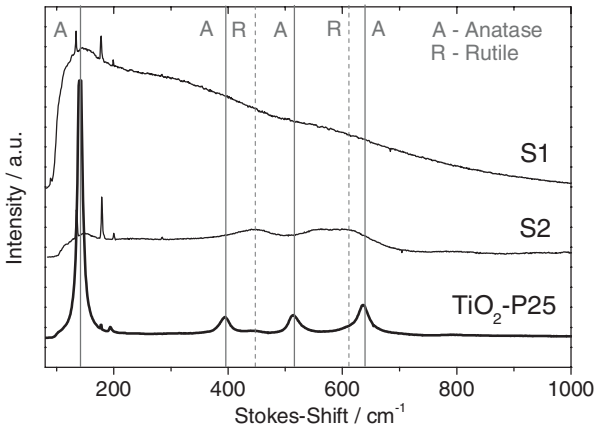

Figure 1 Raman spectra of a crystalline TiO_2-P25-film together with a TCO-like $Nb_{0.03}Ti_{0.97}O_{1.84}$-film (S1) and an isolating $Nb_{0.03}Ti_{0.97}O_{1.91}$-film (S2).

and Nb_xO_y-phases. Figure 1 shows Raman-spectra of a TiO_2-P25 sample together with two Nb:TiO_2-layers prepared at different sputtering-conditions. TiO_2-P25 is a composite material made of Rutile- and Anatase-TiO_2-crystallites of about 20 nm in diameter what was used here for reasons of comparison. The Anatase-modes of the P25-film (d) are strong and dominate in intensity with respect to the Rutile-modes at 447 cm^{-1} and 612 cm^{-1}. The mode positions coincide well with literature values given in Table 2. The spectrum S1 belongs to a Nb:TiO_2-film with the stoichiometry $Nb_{0,03}Ti_{0,97}O_{1,84}$. A clear, ramp-like Raman signal for wavenumbers between 100 cm^{-1} and 800 cm^{-1} can be seen. One significant and two weaker peaks occurred at 145 cm^{-1}, 315 cm^{-1} and 564 cm^{-1}. A 4-mode deconvolution with target-modes that correspond to TiO_2-rutile- and Ti_2O_3-phases gave maxima at 142, 218, 355 and 578 cm^{-1} [29]. The accordance of the first and the two last modes fits roughly between experiment and deconvolution. But, the signal at 564 cm^{-1} may also correspond to an NbO_2-species for which a literature value of 580 cm^{-1} is given (Table 2).

The broadening of the Raman-modes is caused by the small particle size and their interaction with an elastic, non-complete crystalline crystall-lattice, leading to a shortening of the lifetime of vibrational excited states [30]. The Raman spectra of a highly oxidic sputtered film with the stoichiometry $Nb_{0,03}Ti_{0,97}O_{1,91}$ is presented by curve S2. The peak-maxima at 146 cm^{-1}, 447 cm^{-1} and 608 cm^{-1} can be clearly assigned to TiO_2-Rutile literature values (Table 2). Because none of the samples showed a signal at 996 cm^{-1},

Table 1 Composition of $Nb_xTi_{1-x}O_y$-films estimated with elastic recoil detection analysis (ERDA).

deposition conditions		[Nb]/[Ti]	([Nb] + [Ti])/[O]	film composition
O_2: 3.25–3.32 sccm, 400 K	TCO	0.033–0.035	0.539–0.546	$Nb_{0.03}Ti_{0.97}O_{1.84}$
O_2: >3.35 sccm, 400 K	isolator	0.031–0.033	0.523–0.528	$Nb_{0.03}Ti_{0.97}O_{1.91}$
add. annealed 720 K, air		0.030–0.033	0.501–0.515	$Nb_{0.03}Ti_{0.97}O_{1.96}$

Table 2 Raman-modes of expected titanium- and niobium-oxides (Stokes-shift).

material	mode (cm^{-1})	References
TiO_2-anatase	144 (E_g, s); 197 (E_g, w); 399 (B_{1g}, s); 515 (A_{1g}, m); 519 (B_{1g}, s); 639 (E_g, m);	[25]
TiO_2-rutile	143 (B_{1g}, s); 447 (E_g, s); 612 (A_{1g}, s); 826 (B_{2g}, w)	[26]
Ti_2O_3*	238 (A_{1g}, m); 279 (E_g, s); 350 (E_g, m); 465 (E_g, w), 513 (A_{1g}, w); 567 (E_g, w)	[27]
NbO_2*	415 (m), 434 (m), 580 (s)	[19]
Nb_2O_5*	280 (m), 630 (m), 996 (s)	[28]

s – strong, m – medium, w – weak intensity; * – not all modes are shown.

the presence of Nb_2O_5-species can be excluded. The substrate and metallic sputtered films did not show Raman signals at all. Additional annealing of the samples S1 and S2 at 720 K for 1 hour in air changed their Raman spectrum in that way, that sharp signals rose at 143, 388, 513 and 634 cm^{-1}, indicating the formation of TiO_2-Antase in the layers (Fig. 2). The signals of the formerly mentioned Rutile-modes did not change in position and intensity.

From the Raman-modes position the crystallite size in the sample can be determined [31, 32]. By using the empirical correlation given in [31, 32], average particle sizes of about 13 nm and 25 nm for the additionally annealed and of 2 nm and 4 nm for the untreated $Nb_{0,03}Ti_{0,97}O_{1,84}$- and $Nb_{0.03}Ti_{0.97}O_{1.91}$-films, respectively, were estimated.

3.2 The electronic and optical properties of the $Nb_xTi_{1-x}O_y$-films For the reactive magnetron sputtered $Nb_xTi_{1-x}O_y$-films, the oxygen flow-rate was the key-factor for influencing the film properties such as conductivity and transparency. For an oxygen flow-rate below 3.0 sccm opaque metallic- and bronze-like films were obtained, whereas for oxygen flow-rates higher than 3.5 sccm highly transparent but insulating films were deposited. This general behaviour was observed for both, reactively sputtered films with and without niobium as a dopand. Due to the fact that even a small change in the oxygen flow-rate (ΔF_{O_2}: 0.02 sccm) can cause strong changes in the discharge voltage (U_E, Fig. 3), this quantity can be used to control the deposition process sensitively. Figure 3A shows the general dependence of U_E versus the oxygen flow-rate.

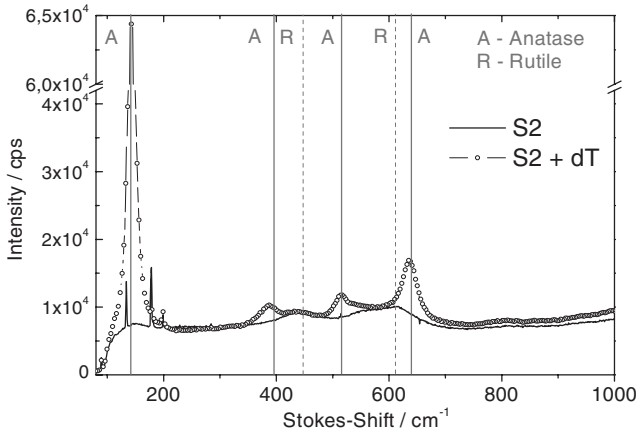

Figure 2 Raman spectra of the sample S2 before ($Nb_{0.03}Ti_{0.97}O_{1.91}$) and after an additional annealing at 720 K for 1 h in air ($Nb_{0.03}Ti_{0.97}O_{1.96}$). Former amorphous areas crystallized out by forming TiO_2-Anatase crystallites.

The variation in U_E is caused by oxygen induced changes in the secondary electron emission coefficient of the target's surface. The secondary electrons themselves are needed to sustain the plasma discharge at the fixed discharge power (200 W). In other words, U_E characterizes the oxidation-status of the targets surface. Transparent and conductive $Nb_{0.03}Ti_{0.97}O_{1.84}$-films can be deposited at the steepest slope of the U_E-curve given in Fig. 3B for discharge voltages between 428 V and 435 V. The average resistivity of these films was $\sim 0.9\ \Omega$ cm for an U_E between 428–432 V and of $\sim 10\ \Omega$ cm for an U_E between 432–435 V. To keep the film deposition reproducible, it is necessary first to condition the target under "metallic" sputter-condition before each run and second to sew on the desired working point/discharge voltage stepwise with an fine tuning in the oxygen-flow rate.

Local inhomogeneities were present in the deposited films (±20% in specific resistivity), which may be caused by the circular plasma-torus and the extraordinary high chemical reactivity between sputtered Ti-atoms and oxygen. Hall-measurements showed that the charge carrier concentration in the $Nb_{0.03}Ti_{0.97}O_{1.84}$-films is about 5.0×10^{20} cm^{-3} high, a value that is comparable to other TCO-materials, like Al:ZnO (Table 3). Assuming one oxygen vacancy per Nb^{5+}-atom in the lattice, as is proposed by Ruiz and Valigi et al. [19, 20], the value of the charge carrier concentration agrees well with niobium-atom density of 9.5×10^{20} cm^{-3}, which was calculated by using the measured doping level (3 at% Nb, chapter 3.1) and the density of TiO_2-Rutile (ρ: 4.25 g cm^{-3}). The Hall-mobility of the charge carriers in the $Nb_{0,03}Ti_{0,97}O_{1,84}$-films is, with values of about 0.9 $cm^2\ V^{-1}\ s^{-1}$, low compared to aluminium-doped ZnO-films, which typically show Hall-mobilities between 20 $cm^2\ V^{-1}\ s^{-1}$ and 100 $cm^2\ V^{-1}\ s^{-1}$ [3, 8, 33]. With increasing charge carrier concentration, the room temperature Hall-mobility decreased, what is a typical behavior of degeneratively doped semiconductors [3]. This is further supported by the observed temperature-dependence of μ_{Hall} (Fig. 4), which shows an increase in the mobility with decreasing temperature. Films sputtered from a pure titanium-target showed more than 10-times lower charge carrier mobilities (Table 3) than the Nb-

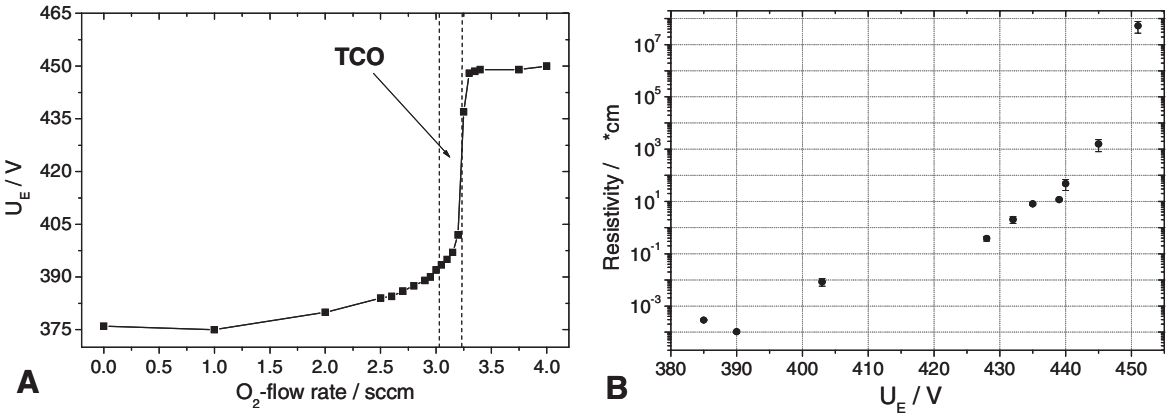

Figure 3 A: Discharge voltage (U_E) as function of the O_2-gas flow rate. The S-shaped curve is a result of an oxidation of the targets surface. B: The specific resistivity of certain $Nb_xTi_{1-x}O_y$-films is plotted against U_E, present during their deposition. TCO-like films were obtained between 428–435 V, what is related to an O_2-gas flow rate of 3.15 sccm to 3.30 sccm.

Table 3 Hall-mobilities (μ_{Hall}) and charge carrier concentrations (n_e) of different TCO-materials.

material	μ_{Hall} ($cm^2\ V^{-1}\ s^{-1}$)	n_e (cm^{-3})	References
$TiO_{1.87}$	0.05	5.0×10^{20}	this work
$Nb_{0.03}TiO_{0.97}O_{1.84}$	0.9	2.4×10^{20}	
Al:ZnO	20–100	5.0×10^{19}	[3, 8]
$Nb_{0.06}Ti_{0.94}O_2$**	25	1.0×10^{21}	[7]

** – epitaxial films prepared by Laser-ablation at 820 K [7].

doped films did. The charge carrier concentration and the conductivity of the $Nb_{0.03}Ti_{0.97}O_{1.84}$-films decreased with decreasing temperature (Fig. 5A and B), which underlines again their semiconductor-like behaviour.

The activation energies for charge transport in the $Nb_{0.03}Ti_{0.97}O_{1.84}$-films were estimated to be 50 meV and 192 meV, respectively. The average transparency for the typically 150 nm thick $Nb_{0.03}Ti_{0.97}O_{1.84}$-films was about 60–80% in the wavelength-region 400 nm to 800 nm and 55–65% for wavelengths between 800 nm and 1200 nm (Fig. 6, neglecting the absorption of the substrate). Films sputtered at higher oxygen flow rates ($Nb_{0.03}Ti_{0.97}O_{1.91}$) and additionally annealed samples (720 K, 1 h air, $Nb_{0.03}Ti_{0.97}O_{1.96}$) showed an increase of transmission (Fig. 6) and their slope of the absorption coefficient, plotted versus the photon-energy, was steeper. This can be understood as a result of a reduced number of bandgap defect states in the films [34]. The band-to-band transition energy (indirect) was estimated to be 3.32 eV for the TCO-like $Nb_{0.03}Ti_{0.97}O_{1.84}$-films. The blue-shift in band-gap energy relative to undoped Rutile-crystallites should mainly

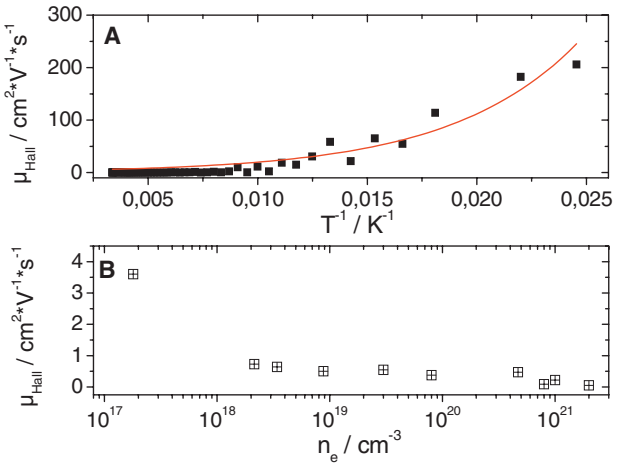

Figure 4 (online colour at: www.pss-b.com) A: Hall-mobility of an $Nb_{0.03}Ti_{0.97}O_{1.84}$-film in dependence on the temperature. B: Plot of the Hall mobility of different $Nb_{0.03}Ti_{0.97}O_y$-films (y: 1.84–1.91) to stress out its dependence on the charge carrier concentration.

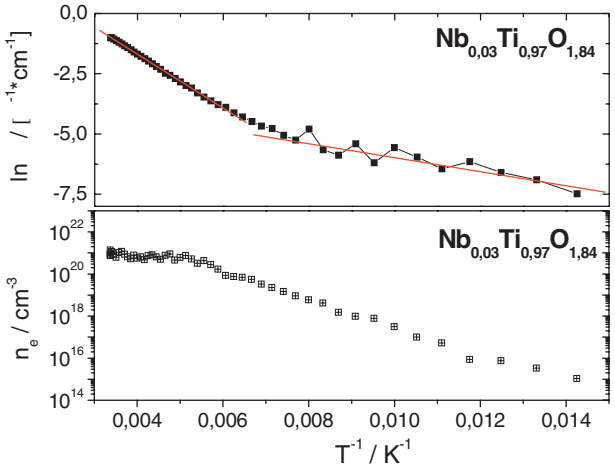

Figure 5 (online colour at: www.pss-b.com) Logarithm of the conductivity ($Nb_{0.03}Ti_{0.97}O_{1.84}$-film) as function of the temperature. The charge transport activation energies were calculated to be 50 meV and 190 meV. The charge carrier concentration in the $Nb_{0.03}Ti_{0.97}O_{1.84}$-film decreased with decreasing temperate, showing its semiconducting behaviour.

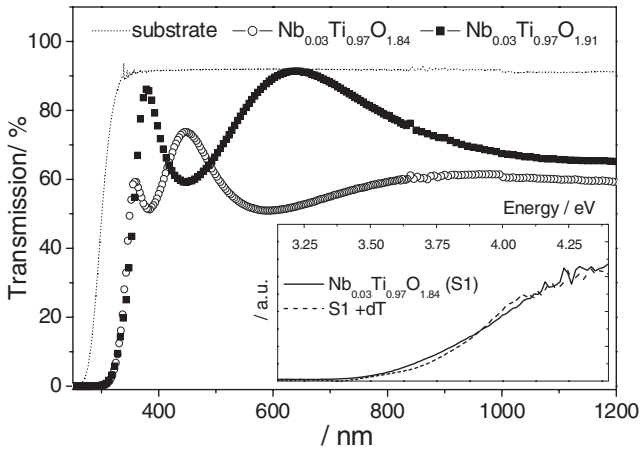

Figure 6 Transmission spectra of a bare glass substrate, a TCO-like $Nb_{0.03}Ti_{0.97}O_{1.84}$-layer and a highly oxidic sputtered $Nb_{0.03}Ti_{0.97}O_{1.91}$-layer. Additional annealing of the $Nb_{0.03}Ti_{0.97}O_{1.84}$-layer (air, 1 h, 723 K) reduces the number of inner bandgap-states, causing a steeper rise of the absorption coefficient. The latter is shown in the inset of Fig. 6, where the absorption coefficient of an origin (S1) and an additionally annealed $Nb_{0.03}Ti_{0.97}O_{1.84}$-film (S1 + dT) is plotted against the energy of incident light.

be caused by the small particle size of about 2–4 nm (chapter 3.1) and the resulting quantum size effects [34].

3.3 Comparison between a standard iZnO/Al:ZnO- and a $Nb_{0.03}Ti_{0.97}O_{1.84}$-window layer To investigate if the new $Nb_{0.03}Ti_{0.97}O_{1.84}$-films can be used as a window layer, thin film solar cells choosen from the same Cu(In,Ga)Se_2- and CdS-deposition-batch were divided into two groups. One group received the standard intrinsic- and aluminium-doped ZnO-window-layer including a nickel:aluminium-contact grid (R_{sheet}: 0.3 Ω cm^{-2}) while the other group received the new $Nb_{0.03}Ti_{0.97}O_{1.84}$-window layer including a titanium-contact grid (R_{sheet}: 48 Ω cm^{-2}). Both groups of solar cells were characterized according to their *I–V*-characteristics in a sun simulator (Table 4 and Fig. 7).

Table 4 Characteristics of standard ZnO- and new $Nb_{0.03}Ti_{0.97}O_{1.84}$-equipped Cu(In,Ga)$Se_2$ solar cells.

window	j_{SC} (mA cm^{-2})	V_{OC} (mV)	FF (%)	η (%)
ZnO	28.0	580	67.4	12.6
	32.7	570	67.8	14.2
	29.0	580	71.7	13.6
	31.2	570	71.1	14.5
Mean	30.5 ± 1.6	570 ± 4	69.5 ± 1.9	13.7 ± 0.7
$Nb_{0.03}Ti_{0.97}O_{1.84}$	8.2	570	39.9	2.1
	11.6	560	39.7	3.0
	10.3	520	39.6	2.0
	8.9	550	38.5	1.9
Mean	9.8 ± 1.3	550 ± 20	38.7 ± 1.3	2.3 ± 0.4

j_{SC} – short circuit current, V_{OC} – open circuit voltage, FF – fill factor, η – solar efficiency, Mean – mean value with standard deviation.

The solar cells prepared with the standard window showed an average short circuit current density of about 30 mA cm^{-2}, an open circuit voltage of 570 mV, fill-factors of about 69%. The mean-efficiency is 13.7% (Table 4). The solar cells equipped with the new window layer showed a reduced mean short circuit current density of 9.8 mA cm^{-2}, an open circuit voltage of 550 mV and fill-factors of about 38%, resulting in an efficiency of only 2.3%. Due to the coincidence in V_{OC} between standard- and modified solar cells, the presence of strong energetic barriers between the CdS-buffer layer and the $Nb_{0.03}Ti_{0.97}O_{1.84}$-front contact can be excluded.

In addition one can deduce that the buffer layer did not degrade during the $Nb_{0.03}Ti_{0.97}O_{1.84}$-sputter process. The strong decrease in j_{sc} in case of $Nb_{0.03}Ti_{0.97}O_{1.84}$-deposited solar cells results foremost from the lower transmission (~−20%) of the $Nb_{0.03}Ti_{0.97}O_{1.84}$-front contact relative to the ZnO-films. But also, a slightly increased charge carrier recombination may be responsible for this.

The first mentioned argument is supported by quantum efficiency measurements (Fig. 7B), where a small light ray is focused near the contact grid so that differences in charge transport may therefore be neglected. The difference in the measured external quantum efficiency (EQE) between both cell types nearly fits with the differences in transmission. In addition, the lower cell efficiency is caused by the less ideal fill-factor of the cells and the higher sheet resistance of the titanium-contact grid. According these points major development efforts are needed.

By fitting the dark *I–V* curves of the solar cells, the diode factor as well as the series and the parallel-resistances in the cell can be calculated by using the following modified Schottky-equation [34]:

$$j(V) = j_0^* \left[e^{\frac{e_0^*(V - j(V)R_s}{nkT}} - 1 \right] + \frac{V - j(V)R_s}{R_p} \quad , \qquad (1)$$

with V the applied voltage, n the diode factor, e_0 the elementary charge, k the Boltzmann constant, T the temperature, R_s the series-resistance and R_p the parallel-resistance. ZnO-equipped Cu(In,Ga)Se_2-solar cells typically showed diode factors of about 2.0, series resistances of about 0.15 Ω cm^{-2} and parallel resistances of about 1500 Ω cm^{-2}. For the $Nb_{0.03}Ti_{0.97}O_{1.84}$-equipped solar cells, n and R_s increased to values of about 2.3 and 3.0 Ω cm^{-2}, respectively, whereas R_p did not change markedly (1400 Ω cm^{-2}). The increased diode quality factor of the $Nb_{0.03}Ti_{0.97}O_{1.84}$-equipped solar cells relative to the ZnO-equipped ones can result from a less ideal band-alignment and from differences in recombination processes at the pn-hetero-junction. The observed increase in the solar cells R_s-value can be explained by the lower conductivity of the $Nb_{0.03}Ti_{0.97}O_{1.84}$-films relative to the ZnO-films and by the higher sheet-

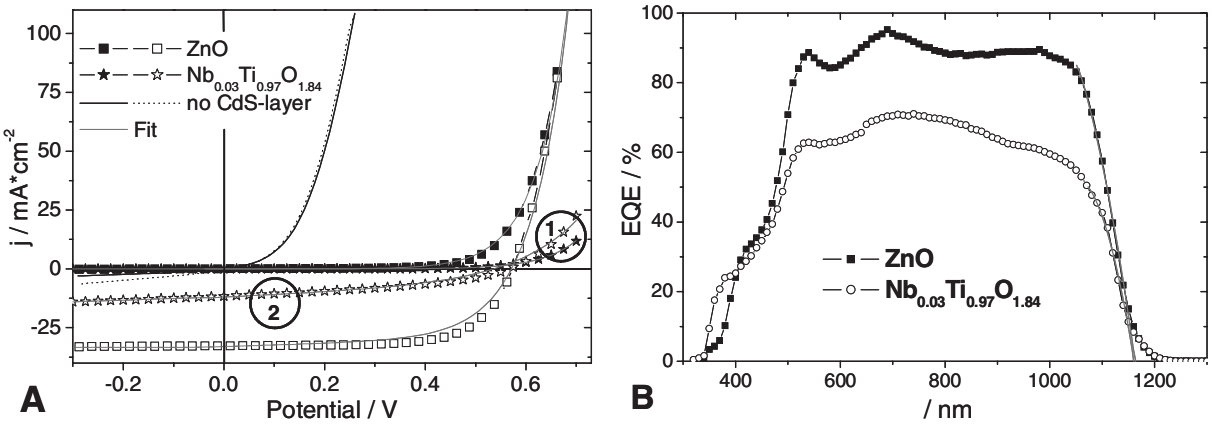

Figure 7 (A) Dark and AM1.5-light *I–V* characteristics of a standard, i:ZnO/Al:ZnO-equipped, $Cu(In,Ga)Se_2$ solar cell (filled and unfilled square, ZnO) together with a $Nb_{0.03}Ti_{0.97}O_{1.84}$-equipped $Cu(In,Ga)Se_2$ solar cell (filled and unfilled star, $Nb_{0.03}Ti_{0.97}O_{1.84}$). The blank and the dotted line in (A) result from an solar cell that was prepared with a $Nb_{0.03}Ti_{0.97}O_{1.84}$- but without a CdS-buffer-layer. Cycle No. 1 – cross-over effect, cycle No. 2 – potential dependent photocurrent collection. (B) Spectral resolved external quantum efficiency of a i:ZnO/Al:ZnO-equipped- and a $Nb_{0.03}Ti_{0.97}O_{1.84}$-equipped $Cu(In,Ga)Se_2$ solar cell.

resistance of the titanium-contact grid. In addition to these points, the $Nb_{0.03}Ti_{0.97}O_{1.84}$-equipped solar cells showed a clear cross-over effect (circle 1, Fig. 7A) and a voltage depended photocurrent collection (circle 2, Fig. 7A). The cross-over effect points out that the current flow through the hetero-junction changed under illumination. A thermally and optically enhanced charge transport within the layers is reasonable due to results of conductivity measurements presented in chapter 3.2 and Fig. 5 together with the finding of a marked photoconductivity of the $Nb_{0.03}Ti_{0.97}O_{1.84}$-layers under UV-light.

The voltage dependent photocurrent collection (circle 2, Fig. 7A) can be a result of a lowered parallel resistance or of an increase in the voltage dependent depletion-zone-width. The first point is apparently not relevant, due to the extracted R_p- and the unaffected V_{OC}-values. The second point can be investigated by estimating an effective charge collection length in the solar cell after fitting the spectrally resolved QE-curves at wavelengths near the absorbers bandgap-energy ($Cu(In,Ga)Se_2$: 1.06 eV). The idea behind this approach is a model given by Gärtner [35], which was simplified by Klenk [36]. The estimated effective charge collection lengths (slope of the QE-onset in Fig. 7B) were with 675 nm higher for the ZnO- than for the $Nb_{0.03}Ti_{0.97}O_{1.84}$-equipped solar cell with an estimated value of 580 nm. Experiments with $Nb_{0.03}Ti_{0.97}O_{1.84}$-equipped solar cells without the CdS buffer layer were not successful. The diode behaviour of the cells breaked down and no photocurrent and no photovoltage could be observed (Fig. 7A).

In experiments repeated after one month's storage in air, the $Nb_{0.03}Ti_{0.97}O_{1.84}$-equipped solar cells showed a slightly higher degradation than the standard ZnO-equipped cells. But, before reliable long term solar cell stability tests can be made, the quality of the $Nb_{0.03}Ti_{0.97}O_{1.84}$-films should be further optimized in order to produce films with similar transparency and thickness like the Al:ZnO-films typically have.

3.4 Discussion The reactively sputtered $Nb_{0.03}Ti_{0.97}O_{1.84}$-films deposited at temperatures below 420 K consist of small, 2–4 nm sized TiO_2-Rutile particles embedded in an amorphous matrix. The fact that the thermodynamically more stable Rutile-phase is created first, can be attributed to the high energy of the sputtered particles that is usually about 5 eV [13]. This is also reported elsewhere [37]. In general, reactive sputtering of crystalline TiO_2-films at temperatures below 500 K is a difficult task. The right relation between the energy of sputtered atoms and the oxygen flow-rate is necessary in order to have a fast crystal-growth and a sufficient adatom mobility on already deposited particles [13, 14, 17]. Due to the observation that only the oxygen- but not the niobium-concentration was affected by the oxygen flow-rate during the film deposition, it seems, that the number of oxygen defect sites is the key-factor for influencing the optical and electrical properties of the $Nb_xTi_{1-x}O_y$-films. Such oxygen defects can be generated first from an insufficient oxygen-concentration during the film growth-process and second from a built-in population of Nb^{5+}-ions into the TiO_2-lattice, which must consequently be neutralized by the surrounding lattice for an overall charge balance. Such neutralisation is thinkable by one oxygen defect site per two Nb^{5+}-ions as well as by one Ti^{4+}-defect site for every four Nb^{5+}-ions or by a generation of additional oxygen-anions at interstitial lattice-positions [19, 21]. The latter point is rather implausible due to the high formation energy of such interstitials [19]. Oxygen defects inside a TiO_x-lattice usually create Ti^{3+}-ions, that are able to release, after thermal or optical ionization, an electron into the conduction band [9]. This can explain first the high charge carrier concentrations in the $Nb_{0.03}Ti_{0.97}O_{1.84}$-films of about 2.4×10^{20} cm^{-3} and second

the temperature dependence of its conductivity. The oxygen deficit in the $Nb_{0.03}Ti_{0.97}O_{1.84}$-films relative to air annealed ones and the observed Raman-signal of Ti_2O_3 species give support for a partial formation of Magneli-phases in the films. Magneli-phases (Ti_nO_{2n-1}) also show high conductivities up to 1500 Ω^{-1} cm^{-1} and a bluish optical appearance [38]. But, typically Magneli-phases show metallic behaviour rather than a semiconducting ones, as it was observed here for the $Nb_{0.03}Ti_{0.97}O_{1.84}$-films.

The high defect concentration in the $Nb_{0.03}Ti_{0.97}O_{1.84}$-films together with the small particle size and the amorphous regions present in the samples can further explain that the charge carrier mobility is two orders of magnitude lower than in sputtered Al:ZnO-films [3]. Especially the last two points give evidence to a grain-boundary limited charge transport. With help of the grain-boundary model of Seto [39], one can deduce the mobility inside the grains (μ_0) from the measured, temperature dependent effective charge carrier mobility (μ_{eff}, Fig. 4) via the equation:

$$\mu_{\text{eff}} = \mu_0 \, e^{-E_B/kT} \quad , \tag{2}$$

where E_B is the thermal activation energy to overcome an energy barrier between two grains, k is the Boltzmann-constant and T the temperature. For the $Nb_{0.03}Ti_{0.97}O_{1.84}$-films μ_0 was calculated to be about 3.5 cm^2 V^{-1} s^{-1}, which is significantly higher than the experimentally measured effective charge carrier mobility (Table 3). Increasing the crystal-size and minimizing the extent of amorphous areas would probably let the mobility and hence the conductivity of the $Nb_{0.03}Ti_{0.97}O_{1.84}$-films increase.

Compared to the data of $Ti_{1-x}Nb_xO_2$ ($x = 0.002-0.2$) films investigated by Furubayashi et al. [7], the $Nb_{0.03}Ti_{0.97}O_{1.84}$-films prepared by reactive sputtering show similar charge carrier concentrations, but the conductivity and the Hall-mobility were markedly lower and the investigated films show rather a semiconducting behaviour than a metallic one. One reason for these discrepancies may be the difference of oxygen content in the films and the therefore increased number of lattice and hence electronic, defects in the $Nb_{0.03}Ti_{0.97}O_{1.84}$-layers. A second reason is attributed to the deposition method itself. The deposition at high temperatures around 820 K produced crystalline $Ti_{1-x}Nb_xO_2$-particles with large sizes, which further reduces the number of grain boundaries in the films. In addition, a pre-ordered $SrTiO_3$-substrate was used instead of amorphous glass substrates in order to obtain epitaxial film growth.

A window layer of a photovoltaic solar cell must accomplish several tasks. First, it has to have a high transparency in the wavelength region where the active layer absorbs light. Second, a sufficiently high conductivity is necessary to ensure an effective charge collection and third, especially for hetero-junctions, the energy-band alignment is crucial with respect to the reduction of interface recombination processes and with respect to achieving high open-circuit voltages. In the so far used Cu(In,Ga)Se_2 solar cells, two different types of energy-band offsets exist [40]. The energy barrier between the conduction band of the CdS-buffer layer and the Cu(In,Ga)Se_2-absorber is a "Spike", whereas the band-offset between the conduction band of CdS- and i-ZnO-front contact is referred as a "Cliff". Typically, the conduction band discontinuities in Cu(In,Ga)Se_2-hetero junctions range about −0.3 and +0.3 eV for the Spike and the Cliff, respectively [40]. In general, a small spike is even beneficial for the solar cell performance, because it increases the inversion-layer at the Cu(In,Ga)Se_2-surface and therefore reduces the interface recombination [40]. It seems that for the $Nb_{0.03}Ti_{0.97}O_{1.84}$-equipped Cu(In,Ga)$Se_2$-solar cells the energy barrier between CdS and absorber differs from the standard cells because of the observed increase in potential dependent charge carrier collection. In addition, the changed charge carrier concentration in the $Nb_{0.03}Ti_{0.97}O_{1.84}$-films relative to the Al:ZnO-films, may also be responsible for changes in the interface of the solar cell's heterojunction which can further explain the reduced effective charge carrier collection lengths. Due to the constancy in V_{OC} between standard- and $Nb_{0.03}Ti_{0.97}O_{1.84}$-equipped solar cells, a high energetic barrier as well as a strongly enhanced recombination between the new interface CdS-buffer layer and $Nb_{0.03}Ti_{0.97}O_{1.84}$-front contact can be excluded.

4 Conclusion Transparent and conductive $Nb_{0.03}Ti_{0.97}O_{1.84}$-films have been prepared by reactive magnetron sputtering at temperatures that allow their deposition on thin film chalcopyrite solar cells with CdS-buffer layer. The energetic and electronic properties of these films, namely the proper energetic position of the conduction band and the high charge carrier density, enables these films to fulfill their role as a window layer in the heterojunction of a Cu(In,Ga)Se_2 solar cell. The open circuit voltage was not affected by the new front contact layer what excludes first the presence of strong energy barriers at the new interface and second strong interfacial recombination. Due to the lower optical transmission (~−20%) and the lower conductivity relative to standard ZnO-window layers, the short circuit current as well as the overall cell efficiency decreased. The distinct cross-over effect and the potential-dependent charge carrier collection in the $Nb_{0.03}Ti_{0.97}O_{1.84}$-based solar cells identify the goals for further optimizations.

The most limiting properties of the $Nb_{0.03}Ti_{0.97}O_{1.84}$-films were the small crystallite size and the inhomogeneous crystallization of the films. By solving these problems, the charge carrier mobility would be increased, due to the reduction of grain-boundaries. This would also be beneficial for the conductivity of the films and for the protection of donor states against oxidation in air.

Acknowledgements Mr. W. Bohne and Mr. P. R. Völz are acknowledged for ERDA-measurements and technical support as well as Mr. S. Brunken is thanked for support with the Hall-measurements.

References

[1] A. L. Dawar, J. Mater. Sci. **19**, 1 (1984).
[2] D. Mergel, Vakuum in Forschung und Praxis **16**, 58 (2004).
[3] K. Ellmer and R. Mientus, Thin Solid Films, DOI: 10.1016/j.tsf.2007.05.084 (2007).
[4] III–Vs Rev., News Update: Technol. Optoelectron. **18**(2), 17 (2005), www.three-fives.com.
[5] H. Gerischer and N. Sorg, Electrochim. Acta **37**, 827 (1992).
[6] P. Spathis and I. Poulios, Corros. Sci. **37**, 673 (1995).
Q. Qu, C. Yan, Y. Wann, and C. Cao, Corros. Sci. **44**, 2789 (2002).
[7] Y. Furubayashi, T. Hitosugi, Y. Yamamoto, K. Inaba, G. Kinoda, Y. Hirose, T. Shimada, and T. Hasegawa, Appl. Phys. Lett. **86**, 252101 (2005).
[8] R. Klenk, FVS-Workshop, Berlin, 2005, Session III, p. 79.
[9] U. Diebold, Surf. Sci. Rep. **48**, 53 (2003).
[10] R. Sanlines, H. Tang, H. Berger, F. Gozzo, G. Margaritondo, and F. Levy, J. Appl. Phys. **75**, 2945 (1994).
[11] Y. Xu and M. A. A. Schoonen, Am. Miner. **85**, 543 (2000).
[12] I. Oja, A. Mere, M. Krunks, R. Nisumaa, C. H. Solterbeck, and M. Es-Souni, Thin Solid Films **515**, 674 (2006).
[13] K. Ellmer, Solid State Phenom. **67/68**, 261 (1999).
[14] J. A. Thornton, J. Vac. Sci. Technol. A **44**, 3059 (1986).
J. A. Thornton and D. Hoffmann, Thin Solid Films **17**, 5 (1989).
[15] H. Wang, T. Wang, and P. Xu, J. Mater. Sci. **9**, 327 (1998).
[16] B. Karunagaran, R. T. R. Kumar, D. Mangalaraj, S. K. Narayandass, and G. M. Rao, Cryst. Res. Technol. **37**, 1285 (2002); Cryst. Res. Technol. **38**, 773 (2003).
[17] P. Löbl, M. Huppertz, and D. Mergel, Thin Solid Films **251**, 72 (1994).
[18] S. M. Lee, D. G. Cahill, and Th. H. Allen, Phys. Rev. B **52**, 253 (1995).
[19] M. A. Ruiz, G. Dezanneau, J. Arbiol, A. Cornet, and J. R. Morante, Chem. Mater. **16**, 862 (2004).
[20] M. Valigi, D. Cordischi, G. Minelli, P. Natale, P. Porta, and C. P. Keijzers, J. Solid State Chem. **77**, 255 (1988).
[21] L. Sheppard, T. Bak, J. Nowotny, C. C. Sorrell, S. Kumar, A. R. Gerson, M. C. Barnes, and C. Ball, Thin Solid Films **510**, 119 (2006).
[22] E. Pehlivan, F. Z. Tepehan, and G. G. Tepehan, Sol. Energy Sol. Cells **87**, 317 (2005).
[23] Vegards Law: A_xB_{1-x}, lattice constant $a = x\,a_A + (1-x)\,a_B$.
[24] C. A. Kaufmann, A. Neisser, R. Klenk, and R. Scheer, Thin Solid Films **480**, 515 (2005).
[25] T. Ohsaka, F. Izumi, and Y. Fujiki, J. Raman Spectrosc. **7**, 321 (1978).
S. P. S. Porto, P. A. Fleury, and T. C. Damen, Phys. Rev. **154**, 522 (1967).
[26] R. S. Katiyar and R. S. Krishnan, Phys. Lett. A **25**, 525 (1967).
[27] S. H. Shin, R. L. Aggarwal, and B. Lax, Phys. Rev. B **9**, 583 (1974).
[28] P. S. Dobal, A. Dixit, R. S. Katiyar, H. Choosuwan, R. Guo, and A. S. Bhalla, J. Raman Spectrosc. **33**, 121 (2002).
[29] Raman-mode devonvolution: Origin, 4-target-modes at 143 cm^{-1} and 612 cm^{-1} (Rutile) and 279 cm^{-1} and 465 cm^{-1} (Ti_2O_3), R-value: 0.986.
[30] M. Ivanda, K. Furic, S. Music, M. Ristic, M. Gotic, D. Ristic, A. M. Tonejc, I. Djerdj, M. Mattarelli, M. Montagna, F. Rossi, M. Ferrari, A. Chiasera, Y. Jestin, G. C. Righini, W. Kiefer, and R. R. Goncalves, J. Raman Spectrosc. **38**, 647 (2007).
[31] S. Kelly, F. H. Pollak, and M. Tomkiewicz, J. Phys. Chem. B **101**, 2730 (1997).
[32] K. R. Zhu, M. S. Zhang, Q. Chen, and Z. Yin, Phys. Lett. A **340**, 220 (2005).
[33] P. Kuppusami, G. Vollweiler, D. Rafaja, and K. Ellmer, Appl. Phys. A **80**, 183 (2005).
[34] R. Memming, Semiconductor Electrochemistry (Wiley-VCH, Weinheim, 2001).
[35] W. W. Gärtner, Phys. Rev. **116**, 84 (1959).
[36] R. Klenk, Polykristalline $CuGaSe_2$-Dünnschichten für die Photovoltaik – Herstellung und Charakterisierung von Absorbern und Heteroübergängen, Dissertation, Fakultät Elektrotechnik, Universität Stuttgart, Germany (1993).
[37] L. V. Hong, N. T. H. Le, N. C. Thuan, N. D. Thanh, N. X. Nghia, and N. X. Phuc, J. Raman Spectrosc. **36**, 946 (2005).
[38] M. Zweynert, H. Döring, J. Garche, K. Enghard, and K. Wiesner, Chemie Ingenieur Technik **7**, 827 (1998).
[39] J. Y. W. Seto, J. Appl. Phys. **46**, 5247 (1975).
[40] R. Klenk, Thin Solid Films **387**, 135 (2001).